Vibrations in materials with granularity

Zeravcic, Z.

Chapter 4

Collective oscillations in bubble clouds

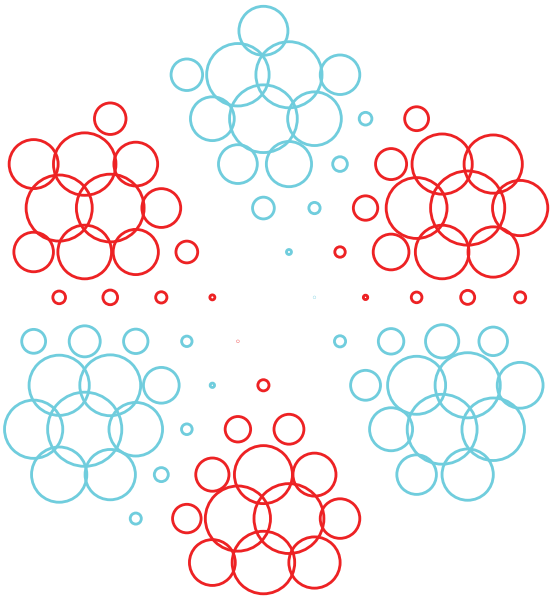

4.1 Introduction

In this Chapter the collective oscillations of a bubble cloud in an acoustic field are theoretically analysed with concepts and techniques of condensed matter physics. More specifically, we will calculate the eigenmodes and their excitabilities, eigenfrequencies, densities of states, responses, absorption, and participation ratios to better understand the collective dynamics of coupled bubbles and address the question of possible localization of acoustic energy in the bubble cloud. The radial oscillations of the individual bubbles in the acoustic field are described by coupled linearized Rayleigh-Plesset equations. We explore the effects of viscous damping, distance between bubbles, polydispersity, geometric disorder, size of the bubbles, and size of the cloud. For large enough clusters, the collective response is often very different from that of a typical mode, as the frequency response of each mode is sufficiently wide that many modes are excited when the cloud is driven by ultrasound. The reason is the strong effect of viscosity on the collective mode response, which is surprising, as viscous damping effects are small for single bubble oscillations in water. Localization of acoustic energy is only found in the case of substantial bubble size polydispersity or geometric disorder. The lack of localization for weak disorder is traced back to the long-rang $1/r$ interaction potential between the individual bubbles. The results of the present Chapter are connected to recent experimental observations of collective bubble oscillations in a two-dimensional bubble cloud, where pronounced edge states and a pronounced low frequency response had been observed, both consistent with the present theoretical findings. Finally, an outlook to future possible experiments is given.

The dynamics of an isolated bubble in an acoustic field is well understood. It can theoretically be well described with the Rayleigh-Plesset equation and extensions thereof [57, 114–116]. The experiments with a single stable sonoluminescing bubble have experimentally confirmed this theory [117].

The situation is much more complicated for *interacting* bubbles. First, the sound emission of an oscillating bubble is felt by the neighboring bubbles in a very large range, as the corresponding Bjerknes potential only decays with $1/r$, where r is the distance between the bubbles [57, 116]. Second, oscillating bubbles attract or reply each other (depending on their mutual size and the driving pressure [75]) thanks to the secondary Bjerknes forces [57, 116]. As we already mentioned in the introductory Chapter of this thesis, interacting bubbles are the genuine case in nature and technology. So further progress in the fundamental understanding of the collective behavior of bubble clouds is desired.

Some progress could be achieved by eliminating the second of the above mentioned complications, namely mutual bubble attraction or repulsion: By exposing air pockets in artificial crevices on a plain surface at well-defined distances to ultrasonic extension waves, [118–120] studied the collective collapse of a bubble cloud with bubbles at fixed positions, thereby decoupling the radial oscillations from the translational dynamics of the coupled bubbles. They found that an extended Rayleigh-Plesset equation – with an extra term taking into consideration the sound emission of

all other bubbles [116,121,122] – well describes the collective dynamics, provided that their mutual distance is large enough. Applying the same trick of trapping gas pockets in artificial crevices of geometrically patterned hydrophobic surfaces, but now driven with only small pressure amplitudes, [123] studied collective modes of coupled oscillating micromenisci in a plane ("two-dimensional bubble cloud"), experimentally finding a resonance at much lower frequency as compared to the one of a single micromeniscus. The origin of the shift is due to the acoustic coupling of the oscillating micromenisci that produces collective modes.

This present work builds on these earlier papers [118,119,123], but aims at a more detailed and fundamental understanding of the spectrum and the response to driving. We will employ concepts and techniques of condensed matter physics which recently experienced a revival in soft condensed matter physics, successfully analyzing vibrational modes in jammed systems (see [33,36,52,124,125]). More specifically, the calculation of the eigenmodes and their excitabilities, eigenfrequencies, densities of states, responses, absorption, and participation ratios turned out to be extremely useful to better understand the dynamics of these jammed systems. We will show in this Chapter that this is also the case for the dynamics of coupled bubbles.

In particular, employing these concepts will allow us to address the question whether *localization* of acoustic energy in bubble clouds is possible. This possibility has been conjectured several times [126–128], but never been analysed with the concepts and techniques of modern condensed matter physics. We want to compare the localization of energy in a bubble cloud with the classical Anderson localization [4] of waves in disordered condensed matter. Here localization refers to the fact that waves, which are extended (like plane waves) in the absence of disorder, can become localized in the presence of disorder. Then a localized state or eigenmode is concentrated around a point in space and has an amplitude that falls off exponentially with the distance from the center. The occurrence of localized eigenmodes in systems that are described with wave-type equations is of a general nature and can be extended to many systems such as sound modes, gravity waves, diffusion on random lattices etc. , [129, 130]. It is therefore a natural question to ask whether localization also plays a major role in collective bubble oscillations, where the disorder can result from both the positional disorder of the bubble centers and from the bubble polydispersity. As we shall see, localization does play some role, but the effects are subtle, partly due to the long-range nature of the bubble-bubble interaction term, which is very different from the short-range interaction common in condensed matter physics. Instead of exponential localization of the modes there is only power law localization.

The phase space to be explored is considerable, being spanned by bubble radius, polydispersity, viscosity, distance between the bubbles, and the underlying structure of the bubble array. For simplicity and for better comparison with experiment, as in [118, 119, 123] we take the positions of the bubbles to be fixed. This however hardly limits the applicability of our approach and our results: Whenever the period of the relevant resonance frequencies is much shorter than the timescale for rearrangements of the bubble cloud, an adiabatic approximation in which the positions of the bubbles are consider fixed, suffices. This applies to many situations of practical

interest.

Already here in the Introduction we illustrate the richness and subtlety of the mode and response behavior of coupled bubble oscillators at various frequencies in Fig. 4.1. The analysis of the full spectrum will reveal both the aforementioned low-energy collective modes with nearby bubbles oscillating in phase and modes with nearby bubbles oscillating in anti-phase that have resonant frequencies larger than those of individual bubbles. This contributes to the nontrivial Density of States (DOS) of the collective modes, which, as common in condensed matter physics, has profound consequences on the response. For better accessibility of the Chapter for the fluid dynamics community, we will explain the origin of these main features along Figure 4.1 in an overview of our results in Section 4.2.

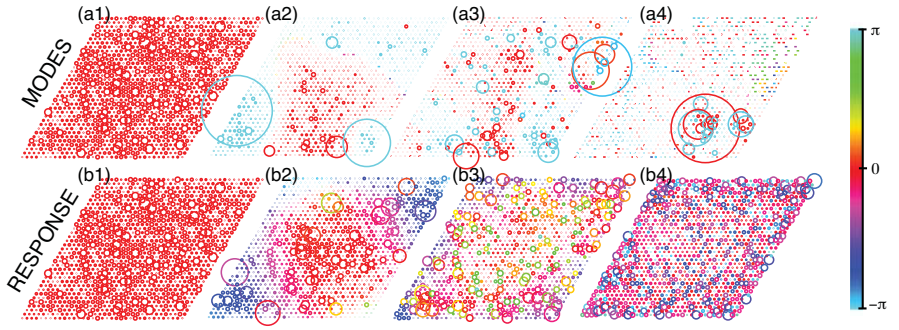

Figure 4.1: Examples of eigenmodes and response fields for a system of $N = 1225$, 20% polydisperse bubbles (with mean radius $R^0 = 5\mu m$), each of which is represented by a circle. The radii of the circles in the plot are proportional to the amplitude of the oscillation and the color shows the phase. (a1-a4) Going from left to right 1st, 7th, 107th and 807th mode, respectively. (b1-b4) Response of the system to uniform driving with the 1st, 7th, 107th, and 807th eigenfrequency, respectively.

The Chapter is organized as follows: Section 4.2 qualitatively discusses the various competing effects and summarizes and physically accounts for the main results. Section 4.3 is dedicated to the formalisms that we used to calculate the spectrum of a cluster of mono- and polydisperse bubbles, calculation of the response of these systems upon driving, and definitions of the quantities we will use to address the properties of both the eigenvibrations and the response. Naturally, this section will be rather technical. In Section 4.4 we present the main results for the case of monodisperse clusters of bubbles positioned in regular ordered arrays. In Section 4.5 we study the effect of disorder introduced by polydispersity and briefly discuss the effects of making the underlying structure random. The last section is dedicated to an outlook on possible experiments to study collective behavior of bubbles in bubbly clouds.

4.2 Qualitative discussion of the physical ingredients and competing effects and main results

The parameter space of coupled bubble oscillations is huge: bubble size and polydispersity, bubble distances, liquid viscosity, thermal diffusivity, surface tension, and density, the corresponding material properties of the gas, and the geometry of bubble arrangements. Clearly, the parameter is far too large to fully explore. So we must restrict ourselves to pinpoint the main trends and to isolate the most important effects. In order to guide the reader's intuition and to set the stage for the further analysis, in this section we will first summarize the most relevant parameters that affect the collective bubble oscillation problem and we will qualitatively summarize the main results.

4.2.1 Single bubble properties: resonance frequency, damping and Q-factor

When surface tension effects are small (as is the case for bubbles larger than a few μm), the resonance frequency Ω^0 of a single bubble with ambient (*i.e.*, static) radius R^0 is the Minnaert frequency [116]

$$\Omega^0 = \sqrt{3p_0^\infty/\rho}\,\frac{1}{R^0}, \tag{4.1}$$

where p_0^∞ is the ambient pressure and ρ the density of the liquid. Its viscous damping rate Γ is given by

$$\Gamma = \frac{\mu}{\rho(R^0)^2}. \tag{4.2}$$

Out of the resonance frequency and the damping rate one can define a quality $Q = \Omega^0/\Gamma$. For a bubble one obtains

$$Q = \frac{\Omega^0}{\Gamma} = \frac{\sqrt{p_0^\infty \rho}}{\mu}\,R^0. \tag{4.3}$$

The Q-factor determines the sharpness of the resonance and response of an oscillator: the larger Q, the more the response is peaked around its natural oscillation frequency Ω^0 (throughout this Chapter we will use the terms *sharpness of the resonance* and *Q factor* interchangeably). An example of this behavior is shown in Fig. 4.1(a1) and (b1): in (a1) we plot the lowest frequency (collective) eigenmode, which is the least damped in the spectrum (see Section 4.3.2 for details). Panel (b1) is a response of the system when uniformly driven with the lowest resonant frequency; the response field is hardly distinguishable from the single-mode behavior in Fig. 4.1(a1). For the rest of the mode examples depicted in Fig. 4.1(a2-a4), the effect of damping is more pronounced, influencing the response, see Fig. 4.1(b2-b4). We come back to the origin of the different behavior at low and high frequencies below.

For a given fluid, the Q-factor can be tuned by the bubble radius. For water at atmospheric pressure, the Q factor is already about 5 for a bubble with a radius of only $1\mu m$. Hence single bubbles of sizes larger than a few μm are weakly damped, *i.e.*, are sharp resonators: the effect of viscosity is small.

4.2.2 Bubble-bubble interactions

The coupling of bubble-bubble oscillations is mediated through the pressure field, which falls off inversely proportional to the distance from an oscillating bubble. This makes the interaction term very different from the short-ranged (near-neighbor-like) interactions that one usually encounters in condensed matter physics: here the interactions are long-ranged, and each bubble interacts with many others. This has several important consequences, one of which is that it appears to suppress the classical Anderson localization with exponentially decaying eigenmodes (see Section 4.5.3 for details). An example of this behavior is shown in Fig. 4.1(a4) where we depict a high-frequency eigenmode of a strongly disordered system (20% polydispersity in the static bubble radii, see Section 4.5.2): compared to high-frequency modes in other (standard) systems described by the wave equation, this mode does not only have a group of bubbles oscillating, but rather a small amplitude background coupled to it.

Other important implications are that the bubble-bubble interactions are never small in large clouds, as each bubble feels many others, and that the strength of the interactions, *i.e.*, *interaction parameter* K, is essentially tuned by varying the ratio:

$$K = \frac{\langle R^0 \rangle}{d}, \tag{4.4}$$

where $\langle R^0 \rangle$ is the average static bubble radius and d the average distance between bubbles (cf. [118]).

4.2.3 The Density of States (DOS)

The presence of interactions between the bubbles will lead to collective modes (like the ones in Fig. 4.1(a1-a4)), which we can label with their resonance frequency. Like any damped harmonic oscillator, each mode will have a Lorentzian response curve whose width in frequency is of order $1/Q$. An important quantity for a large array of bubbles is the Density of States (DOS), $D(\omega)$. For a cloud of N bubbles, $ND(\omega)\mathrm{d}\omega$ is the number of modes with resonance frequency between ω and $\omega+\mathrm{d}\omega$. In condensed matter theory, the DOS is quite important for determining response properties. However, we are not aware of any previous systematic study of the DOS for collective bubble oscillations.

4.2.4 Excitation field

In this study, we will focus the analysis of the response to the case in which the bubble oscillations are driven by a homogeneous pressure field. This is the case most rele-

vant for the patterned surface experiments, in which the wavelength of the sound is much larger than the sample size. Results for spatially dependent pressure fields are in principle accessible by our analysis, but we will not explored them here.

This type of driving leads to an averaging, weighted by the susceptibility of a mode to in-phase excitation. Modes with lots of neighboring bubbles oscillating in anti-phase are driven much less effectively than modes with more oscillations in phase. Therefore, the fact that all bubbles are driven with the *same* phase, has important implications for the response (examples shown in Fig. 4.1(b1-b4)).

4.2.5 The effect of viscous damping and number of bubbles on collective dynamics

We already saw above that since the single-bubble Q-factor is large, viscous effects on single bubble oscillations are typically small. But this is not necessarily so for collective response. In the simplest case, the Q factor of collective modes is not very different from that of a single bubble, so that its frequency response has a width of order $1/Q$. Actually, if we excite an array of N bubbles by a frequency ω, we will only observe single-mode-like response if there are no other modes within a frequency window of order $1/Q$ around ω. In other words, we will have

$$\begin{aligned} &\text{single mode response for} \quad ND(\omega)/Q \lesssim 1, \\ &\text{multi-mode response for} \quad ND(\omega)/Q \gtrsim 1. \end{aligned} \tag{4.5}$$

Clearly, even though the quality factor Q may be large, the sharpness of the individual mode resonances competes with the increase in number of modes N when the cloud gets larger. Moreover, this effect is strongly dependent on the shape of $D(\omega)$: for low frequencies, where $D(\omega)$ is found to be small, it is possible to observe single collective mode response even for reasonable values of N (*e.g.* mode in Fig. 4.1(a1) vs. response in Fig. 4.1(b1)), but for relatively high frequencies, where $D(\omega)$ is large, it is virtually impossible to see single-mode behavior in response (*e.g.* modes in Figs. 4.1(a3-a4) vs. response in Figs. 4.1(b3-b4)). So even though the damping *itself* is small, in the latter case the *effect* of damping is large, through the overlap of the modes. These considerations also affect the possibility to see localization effects of modes, accompanying the discussion in Section 4.2.2 .

4.2.6 Polydispersity

In experiments, bubbles have different static radii, and hence have different individual bubble resonance frequencies. This is actually the most important source of disorder in this system, because bubbles which have similar single-bubble resonances are resonantly coupled, those which have different ones are effectively only weakly coupled. Consequently, even the introduction of polydispersity as small as a few percent in an ordered bubble arrays will turn out to destroy most of the coherent collective modes of the ordered system. Note also that because of the long-range pressure-mediated interaction, bubbles which are relatively far away but which have similar

single bubble resonant frequencies can exhibit strong effective coupling. As a result, the most important factor determining the spectrum is the polydispersity of the bubbles.

As we shall see, the strongly disordered modes are mostly found at higher frequencies, where the $D(\omega)$ is also large (see Figs. 4.1(a3-a4)). In view of Eq. (4.5), upon driving we will typically observe multi-mode response in this frequency range. The averaging over many modes will turn out to wash out much of the disorder in the individual modes: the average response is more coherent than one might have expected, as it turns out to be concentrated at the *edges* of the sample, like in Fig. 4.1(b4). This pronounced response of the bubbles at the edge of the bubble cloud qualitatively resembles the experimental observations of [118, 119], where the phenomenon had been called "shielding" of the inner bubbles. (Note however that in [118,119] the bubbles are oscillating in the non-linear regime so that no quantitative agreement can be expected.)

In line with the above arguments, the lowest frequency modes are those where many bubbles oscillate mostly in phase, Fig. 4.1(a1). These modes are less sensitive to the disorder, and moreover, since the low-frequency density of states is very small, upon driving these modes can be observed as isolated modes. The existence of a low frequency collective response is qualitatively consistent with the experimental observation of [123], who found the most pronounced frequency response of collectively oscillating micromenisci around 150 kHz, though the resonance of a single micromeniscus was around 800 kHz.

In this Chapter, we will only study bubble size distributions which are relatively well peaked, *e.g.* like a Gaussian distribution with a width up to 20%, as this appears to be the experimentally most relevant case. We have also explored distributions with power law tails for small radii (like the Wigner distribution), as well as uniform distribution of finite width, and the obtained results are qualitatively similar with the Gaussian ones.

4.2.7 Influence of geometry and geometric disorder

Geometric disorder, *e.g.* due to randomness in the placement of bubbles, appears to have a relatively unimportant effect, provided that bubbles are never extremely close to each other. We in fact see little difference between various ordered bubble arrays (square, hexagonal, rhombic) and disordered bubble arrangements. This appears to be due to the long-range pressure-induced interaction, which makes the coupling quite insensitive to details of the local geometry.

4.2.8 Effect of dimensionality

In this Chapter, we focus on two-dimensional bubble arrays, both because of the relevance to the recent experiments and because the modes and response are easier to illustrate in two dimensions. We already saw above that because of the long-ranged

interactions, the local geometry hardly matters. Likewise, many of our results will carry over to three-dimensional arrays.

4.2.9 Localization

What sets our system apart from the usual systems displaying localization effects, is the long-range nature of the interaction. We do see localization-like behavior in the individual modes in quantities like the participation ratio, especially for extremal bubbles at large polydispersity, but as we shall detail in Section 4.5.3 of this Chapter, due to the long-range coupling between the bubbles, there is no true exponential localization of the eigenmodes (as already mentioned in Section 4.2.2). Localization effects that we observe play a limited role in the response: These modes are mostly found in a frequency range where multi-mode averaging already washes out many of the disorder effects on individual modes.

4.3 Oscillations of the bubbles

4.3.1 Extended Rayleigh-Plesset equation with driving

The dynamics of interacting bubbles in a cluster can be described with the extended Rayleigh-Plesset equation (see *e.g.* [118, 119, 121, 122]):

$$R_i\ddot{R}_i + \frac{3}{2}\dot{R}_i^2 = \frac{1}{\rho}\Big[\Big(p_0^\infty + \frac{2\sigma}{R_i^0} - p_v\Big)\Big(\frac{R_i^0}{R_i}\Big)^{3\kappa} - \frac{2\sigma}{R_i} + p_v - 4\mu\frac{\dot{R}_i}{R_i} - (p_0^\infty - P_a\sin(\omega_d\cdot t))\Big] - \sum_{j\neq i}\frac{R_j^2\ddot{R}_j + 2R_j\dot{R}_j^2}{r_{ij}}, \quad (4.6)$$

where $R_i(t)$ is the radius of the i^{th} bubble and R_i^0 its static value, ρ is the density of the surrounding liquid, σ is the surface tension, μ is the viscosity, P_a is the pressure driving amplitude, p_0^∞ is the ambient pressure, p_v is the vapor pressure and r_{ij} the distance between the center of the i^{th} and the j^{th} bubble. Since the sizes of bubbles we are going to treat in this study are small (of order a few μm) compared to the thermal diffusion length on the oscillation time scales, we will assume that the gas inside the bubble follows an ideal gas law, modeled with the polytropic coefficient $\kappa = 1$ ([114], [131]). For simplicity we will neglect the pressure of the liquid vapor (for water at 20^oC it is only 0.023atm).

Small driving limit

In the limit of small driving, $P_a \ll p_0^\infty$, Eq. (4.6) can be linearized about the static values R_i^0. This results in a set of coupled damped linear oscillators ([132]. Switching

to dimensionless variables by substituting $R_i = R_i^0(1+q_i)$ in (4.6), we get:

$$\ddot{\tilde{q}}_i(t) + \sum_{j\neq i} \frac{\sqrt{R_j^0 R_i^0}}{r_{ij}} \ddot{\tilde{q}}_j(t) + \frac{4\mu}{\rho(R_i^0)^2}\dot{\tilde{q}}_i(t) + (\Omega_i^0)^2 \tilde{q}_i(t) = \frac{P_a}{\rho(R_i^0)^2}\left(\frac{R_i^0}{\langle R_i^0\rangle}\right)^{1/2} \sin(\omega_d \cdot t), \quad (4.7)$$

where $\tilde{q}_i(t) = \left(\frac{R_i^0}{\langle R_i^0\rangle}\right)^{5/2} q_i(t)$ is a rescaled displacement of the i^{th} bubble to make the equation symmetric in the bubble indices i and j, and ω_d is a driving frequency. The brackets $\langle\cdot\rangle$ denote an average over the bubble size distribution. We also used the fact that

$$(\Omega_i^0)^2 = \frac{3p_0^\infty}{\rho(R_i^0)^2} + \frac{4\sigma}{\rho(R_i^0)^3}, \quad (4.8)$$

is simply the (squared) single-bubble resonance frequency, *i.e.*, the resonance frequency of each individual bubble i in the absence of damping and of interactions with any of the other bubbles. This equation generalizes that of (4.1) given in the introduction; as remarked there, the surface tension term is small for bubbles of radius larger than several μm.

Eq. (4.7) is the linearized Rayleigh-Plesset equation with damping, coupling and driving that is the starting point for our calculations. For simplicity we can rewrite Eq. (4.7) in matrix form:

$$\hat{C}|\ddot{\tilde{q}}(t)\rangle + \hat{\zeta}|\dot{\tilde{q}}(t)\rangle + \hat{\Omega}|\tilde{q}(t)\rangle = |P\rangle \exp(-\imath\omega_d t), \quad (4.9)$$

where we used a quantum mechanics-like notation $|\tilde{q}\rangle$ for the vector that contains all the individual displacements $\tilde{q}_i$ of the bubbles. $\hat{C}$ is a symmetric coupling matrix that has diagonal elements $[\hat{C}]_{ii}$ equal to 1 and off-diagonal elements $[\hat{C}]_{ij}$ equal to $\sqrt{R_i^0 R_j^0}/r_{ij}$. $\hat{\zeta}$ is a diagonal friction matrix with elements $[\hat{\zeta}]_{ii} = 4\mu/(R_i^0)^2\rho$, while the matrix $\hat{\Omega}$ is a diagonal matrix whose elements are simply the square of the single-bubble resonant frequencies, $[\hat{\Omega}]_{ii} = \Omega_i^2$. The driving term on the right hand side is the vector $|P\rangle$ whose elements are $P_i = P_a/(\rho(R_i^0)^2)\cdot(R_i^0/\langle R_i^0\rangle)^{1/2}$. Depending on the presence of polydispersity in our system, the approach to solving the matrix Eq. (4.9) numerically differs. Therefore we will address each case separately.

4.3.2 Spectrum of the system

Monodisperse system

When the initial bubble sizes are all the same, $\hat{\zeta} = \zeta\hat{1}$, $\hat{\Omega} = \Omega_0^2\hat{1}$ and P_i is the same for all the bubbles. To find all the resonant frequencies of the system, we need to solve the homogeneous equation, *i.e.*, without the driving term. We assume a solution of the form $|\tilde{q}(t)\rangle = |u\rangle\exp(-\imath\omega t)$. Substituting this solution into Eq. (4.9) without the driving, we can rewrite the equation in the eigenvalue form:

$$\hat{C}|u\rangle = \left(\frac{\Omega_0^2 - \imath\omega\zeta}{\omega^2}\right)\hat{1}|u\rangle. \quad (4.10)$$

Let us first consider the eigenvalue equation without the damping (*i.e.*, $\zeta = 0$), and denote its eigenvalues by $\tilde{\omega}_i$. These eigenvalues are real, and so are the corresponding eigenmodes $|u_i\rangle$. The latter means that all the bubbles oscillate either in-phase or in anti-phase (corresponding to a phase difference of π). We see that these eigenmodes are also the eigenmodes of the damped case ($\zeta \neq 0$) in Eq.(4.10) (this is valid only for monodisperse systems), while the eigenvalues become the complex frequencies:

$$\omega_i^{\pm} = -\frac{\imath\zeta\tilde{\omega}_i^2}{\Omega_0^2} \pm \frac{\tilde{\omega}_i\sqrt{4\Omega_0^4 - \zeta^2\tilde{\omega}_i^2}}{2\Omega_0^2}. \tag{4.11}$$

The real part of this solution corresponds to resonant frequency of the mode, and the imaginary part is the damping of the resonance (widths of the Lorentzians, $1/Q$). We choose for resonant eigenfrequencies the positive solutions, *i.e.*, the ω^{+1}.

In general, eigenmodes $|u\rangle$ are complex vectors, and the imaginary part describes the phases with which bubbles oscillate. Only in the case of monodisperse bubbles $Im(|u\rangle) \equiv 0$ and consequently bubbles oscillate in phase or anti-phase.

Polydisperse system

In the case when the static bubble radii R_i are not the same, *i.e.*, $R_i^0 \neq R_j^0$, the equation of motion for the system becomes more complicated to solve. In cases like these it is numerically convenient to go to (larger) phase space, and search for the solution there. Eq. (4.9) without the driving will be rewritten in the following way:

$$\hat{\tilde{C}}\dot{y} + \hat{\tilde{\Omega}}y = 0, \tag{4.12}$$

where

$$y = \begin{bmatrix} \dot{\tilde{q}} \\ \tilde{q} \end{bmatrix}; \quad \hat{\tilde{C}} = \begin{bmatrix} 0 & \hat{C} \\ \hat{C} & \hat{\zeta} \end{bmatrix}; \quad \hat{\tilde{\Omega}} = \begin{bmatrix} -\hat{C} & 0 \\ 0 & \hat{\Omega} \end{bmatrix}. \tag{4.13}$$

The new variable y is a vector in the phase space formed out of the degrees of freedom $\tilde{q}$ and their velocities $\dot{\tilde{q}}$. A solution has the form $y = \bar{\Phi}e^{-\gamma t}$, where the set $\{\gamma_i\}$ are the eigenvalues of $\tilde{C}^{-1}\tilde{\Omega}$, and the corresponding (complex) eigenvectors $\{\bar{\Phi}_i\}$ satisfy the orthogonality relation $\bar{\Phi}_i^T\tilde{C}\bar{\Phi}_j = 0$, for $i \neq j$. Since $\dot{y} = -\hat{\tilde{C}}^{-1}\hat{\tilde{\Omega}}y$, we again arrive at the familiar eigenvalue problem:

$$\hat{\tilde{C}}^{-1}\hat{\tilde{\Omega}}\begin{bmatrix} \Phi^{(1)} \\ \Phi^{(2)} \end{bmatrix} = \gamma\begin{bmatrix} \Phi^{(1)} \\ \Phi^{(2)} \end{bmatrix}. \tag{4.14}$$

The imaginary parts of the eigenvalues $\{\gamma_i\}$ are the resonant frequencies, and the real parts are the damping rates[2].

[1] We note in passing that it is easy to work out the above equations by hand for the instructive case of a system of two bubbles. In this case the matrix $\hat{C}$ has off-diagonal terms due to the pressure-coupling. One finds a lower-frequency in-phase mode and a higher-frequency anti-phase mode, which demonstrates a general observation of Section 4.1.

[2] The formalism presented in this Subsection can, of course, also be used for treating the monodisperse systems. The only advantage of the monodisperse approach, described in Subsection 4.3.2, is the

4.3.3 Response of the system to harmonic driving

Driving of the monodisperse system

We are interested in the long-time limit response of the system when driven with a real frequency ω_d. The following formulae are valid for arbitrary real frequency ω_d, although in most of our presented results, we will set ω_d to the resonant frequencies of the system. We proceed by substituting the solution $|\tilde{q}\rangle = |W\rangle e^{-\imath\omega_d t}$ into the Eq. (4.9), which then gives us:

$$(-{\omega_d}^2\hat{C} - \imath\omega_d\zeta\hat{1} + \Omega^2\hat{1})|W\rangle \equiv \hat{\Xi}|W\rangle = |P\rangle. \tag{4.15}$$

To find the response vector we can act on the driving amplitude vector with $\hat{\Xi}^{-1}$. For every driving frequency we have $|W(\omega_d)\rangle$ and these vectors are complex because of the presence of damping. The response of the system written in terms of the eigenvectors of the undriven system is:

$$|W(\omega_d)\rangle = \sum_{j=1}^{n} \frac{\langle u_j|P\rangle}{-{\omega_d}^2(\Omega^2/\tilde{\omega}_i^2) - \imath\omega_d\zeta + \Omega^2}|u_j\rangle. \tag{4.16}$$

According to this equation, the response of the system can be thought of in terms of the sum of many independent damped harmonic oscillators (the modes), each one of which has a response given by the factor in the denominator. This is precisely the picture which underlies the discussion of Section 4.2.5 of the distinction between the single-mode response and the multi-mode response. Moreover, the extent to which each mode is excited, is given by the overlap $\langle u|P\rangle$; as discussed below, we will refer to it as the 'excitability' of a mode. Since $|P\rangle$ is a vector with only positive items, this excitability is largest for the modes where all bubbles oscillate in phase, and zero for perfectly antisymmetric modes. Cf. the discussion in Section 4.2.4.

Driving of the polydisperse system

We now apply the driving $\tilde{P}(t)$ to the coupled polydisperse bubble system eq. (4.12),

$$\hat{\tilde{C}}\dot{y} + \hat{\tilde{\Omega}}y = \tilde{P}, \text{ where } \tilde{P}(t) = \begin{bmatrix} 0 \\ P(t) \end{bmatrix}. \tag{4.17}$$

To find the response, we need to go to the undriven eigenbasis. The calculation is tedious, but the final form is a straightforward generalization of Eq. (4.16) for the monodisperse case,

$$|W(\omega_d)\rangle = \sum_{j=1}^{2n} \frac{\langle\Phi_j^{(2)}|P\rangle}{\gamma_j - i\omega_d}|\Phi_i^{(2)}\rangle. \tag{4.18}$$

As already mentioned above, it is convenient to introduce the *excitability* in connection with the driving — it describes the overlap between the eigenmode $|u_i\rangle$ of

dimensionality of the solution space: instead of searching for N solutions in $2N$-dimensional space, we are searching it in N-dimensional space.

the system ($|\Phi_i^{(2)}\rangle$ for the polydisperse system) and the driving amplitude vector $|P\rangle$, *i.e.*, $\chi_M^i = \langle u_i|P\rangle$ ($\chi_M^i = \langle\Phi_i^{(2)}|P\rangle$). This quantity tells us if an eigenmode can be excited when the system is driven with a certain resonant frequency. Keep in mind, however, that the weight of an eigenmode in the response is also determined by the resonance curve factor (*e.g.* Eq. (4.16)) and by the interference between modes. We will also present the *response excitability*, which represents the overlap between the response vector and the driving amplitude $\chi_R^i = \langle W(\omega_d)|P\rangle$, as well as *absorption*, which is defined as the dissipated energy during one period of driven oscillation and given by the imaginary part of the overlap of the response and driving vectors (absorption $\sim \int_0^{2\pi/\omega} dt Re(\langle P|e^{i\omega t})Re(|W\rangle) \sim Im(\langle P|W\rangle)$).

4.3.4 Localization of vibrations

We will now explore the localization behavior of the eigenvectors of the system and of the response to driving. A standard way to explore this is by looking at the behavior of the so-called participation ratio $P(\omega)$, which is defined as follows:

$$P(\omega_i) = \frac{1}{N}\frac{(\sum_j |v_i^j|^2)^2}{\sum_j |v_i^j|^4}. \tag{4.19}$$

Here the $|v_i\rangle$ are either the eigenmodes $|u_i\rangle$ of the system ($|\Phi_i^{(2)}\rangle$ for the polydisperse system), or the response vectors $|W(\omega_d^i)\rangle$. If $P(\omega_i)$ is of order 1 it means that the mode (response) is extended, and if it is of order $1/N$ the mode (response) is normally called localized. However, we will later show that due to the long-ranged interactions, this picture is over-simplified.

4.4 Results: Monodisperse bubbles on a lattice

Although in experiments bubble polydispersity is always present, in the interest of developing intuition about the system we first consider an "idealized" case of monodisperse bubbles on a lattice.

4.4.1 Undriven system

As explained in Section 4.1, we perform numerical simulations of clusters of bubbles, whose dynamics is described with the linearized extended Rayleigh-Plesset Eq. (4.7). Most of the presented results are for system sizes $N \sim 1000$ bubbles in 2D. We study some of the behavior for system sizes $N \sim 10000$ to check for finite size effects. Parameters that we use in simulations are: *damping constant* $\mu = 2\cdot 10^{-3} Pa\,s$, *density of water* $\rho = 10^3 kg/m^3$, *surface tension* $\sigma = 0.073 N/m$, *atmospheric pressure* $p_{atm} = 101.325 kPa$, *static bubble radius* $R_0 \approx 5\mu m$ and *pitch* $d = 200\mu m$, and we explore three different geometries — *rhombic, square and hexagonal*. With these parameters Eq. (4.8) gives a single bubble resonant frequency $\Omega^0 \approx 4 MHz$. Frequencies

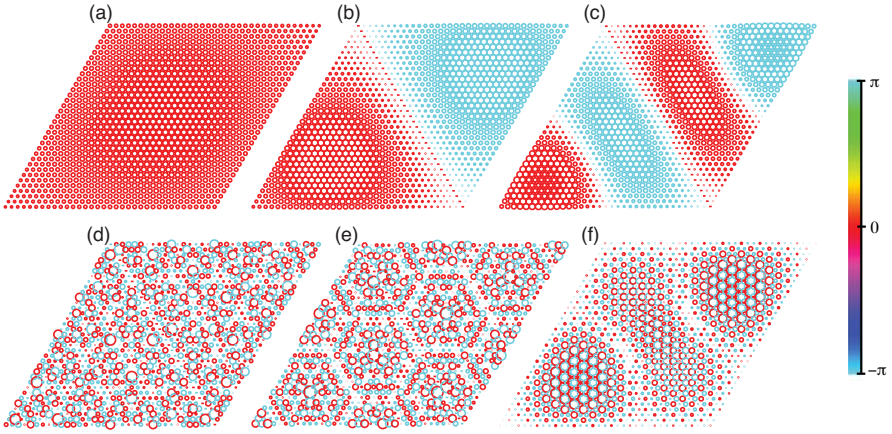

Figure 4.2: Six eigenmodes of the undriven monodisperse 2D bubble cluster. For this illustration we chose (going from left to right in rows) the 1st, 3rd, 5th, 9th, 1128th and 1218th mode of the system with 1225 bubbles in rhombic geometry. The radii of the circles in the plot are proportional to the amplitude of the oscillation and the color shows the phase. Note how in the eigenmodes bubbles oscillate either in phase or in antiphase.

will be plotted in units of Ω^0. The corresponding values of the sharpness of the resonances Q, defined in (4.3), and the interaction parameter K, defined in (4.4), are then $Q_0 \simeq 25$ and $K_0 = 1/40$ (we label these reference values with a subscript 0). These quantities will be different when we consider polydisperse systems in Section 4.5.

Spectrum

Starting from Eq. (4.9), we solve the undriven eigenvalue problem, and obtain eigenmodes and eigenvalues. A few of the obtained eigenmodes (from different parts of the spectrum) are shown in Fig. 4.2. The size of the bubbles is proportional to the amplitude of the oscillation and the color shows the phase. Note how, in agreement with the earlier analysis in Section 4.3.2, in the eigenmodes bubbles oscillate either in phase or in antiphase, giving the modes their plane-wave like structure. Although different arrangements of the bubbles (rhombic, hexagonal,...) naturally have different symmetry axes, the general features of the mode profile remains robust, as already indicated in 4.2.7.

A histogram of the resonant frequencies (real parts of the eigenvalues), *i.e.*, the density of states (see Section 4.2.3), for different system sizes in rhombic geometry is shown in Fig. 4.3(a) in both linear (main panel) and semi-logarithmic (inset) scale. There is a pronounced peak in the spectrum at the single bubble resonant frequency. As in [123], we also observe resonant frequencies much lower in the spectrum, whose origin lies in the acoustic coupling of the bubbles. Some of these collective low-

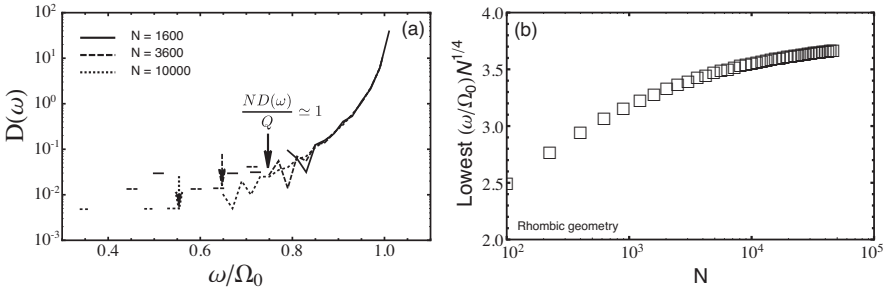

Figure 4.3: (a) Density of states for the 2D monodisperse bubble cluster in rhombic geometry on a log-linear scale. Different curves represent different system sizes. Note the pronounced peak in the spectrum at the single bubble resonant frequency. As mentioned in Section 4.1, due to the coupling between the modes, there are resonant frequencies in the spectrum lower than the single bubble one. Arrows mark the value in the DOS, where the response changes from single-mode to multi-mode one (as defined in Subsection 4.2.5). (b) Scaling of the lowest frequency mode with the increase of the system size. The value of the lowest frequency is rescaled with $N^{1/4}$ to emphasize the asymptotic approach to a constant value in the thermodynamic limit.

frequency modes are depicted in Fig. 4.2(a-c). The arrows in the inset of Fig. 4.3(a) mark the crossover from the single-mode behavior ($ND(\omega)/Q \lesssim 1$) at low frequencies to multi-mode response at higher frequencies. Clearly, for these parameters only one or a few isolated low-frequency modes can be observed in response.

Fig. 4.3(b) shows the finite size effects for the lowest frequency mode, where all bubbles oscillate in phase, and the mode is of course of the size of the system. It is damped the least and scales with the system size as $\omega^2_{lowest} \sim 1/L = 1/N^{1/2}$. This behavior is different from the usual $\omega^2_{lowest} \sim 1/L^2$ scaling in systems described by the wave equation, and originates in the long-range interaction of the bubbles in a cluster[3]. To emphasize the finite size effects we rescale the lowest frequency with $N^{1/4}$ in this figure. Note that systems with $N \sim 1000$ are large enough to capture the essential behavior of the bubble clusters. As in the case of modes, the geometry does not play a significant role (see also Section 4.2.7).

Mode participation ratio

Examples of eigenmodes presented in Fig. 4.2 indicate an extended nature (they are spanning the system). To quantify this behavior, for every eigenmode we calculated the participation ratio defined in Section 4.3.4. This result is shown in Fig. 4.4 for different system sizes and rhombic geometry at the resonant frequency of each mode.

[3]The way to understand this scaling is as follows: Starting from Eq. (4.10), in which we can ignore the damping, and noting that the lowest mode is approximately uniform, we see that in the large-N limit the scaling-structure of the equation is such that $\omega^2 \int_0^L r\mathrm{d}r(R_0/r) \sim \omega^2 L \sim \Omega_0^2$. Hence $\omega \sim L^{-1/2} \sim N^{-1/4}$.

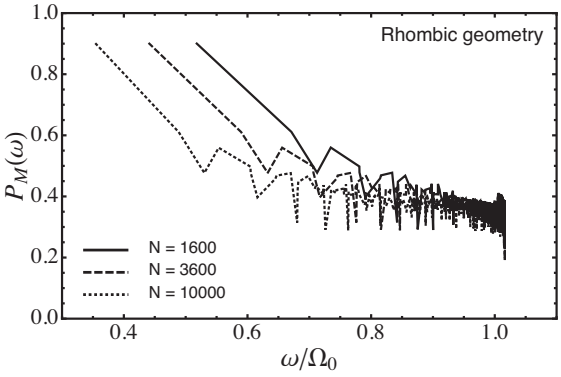

Figure 4.4: Participation ratio of the eigenmodes as a function of the rescaled resonant frequency. Data points are joined by lines for clarity. Different curves represent different system sizes, and the geometry we use is rhombic. Eigenmodes of the monodisperse system are collective plane-wave like modes that span the system and are of extended nature.

Except for the lowest frequency modes, that are extended throughout the system ($P_M(\omega) \sim 1$) the rest of the modes form a plateau with an average $P_M(\omega) \sim 0.4$. In this idealized case of monodisperse bubble clusters, there are no truly localized eigenmodes (modes where the motion is localized on a single bubble or a small group of bubbles), only plane-wave like collective modes. This behavior is independent of the geometry of the problem.

4.4.2 Driven system

As stated in the Section 4.2.5, the analysis of the response to driving presents us with an unexpected effect, namely the *effective damping*, which washes out features in the response. In this Subsection we present additional details and results.

Response participation ratio and response excitability

A few characteristic examples of the response of the system to uniform driving with resonant frequencies (Eq. (4.16)) are shown in Fig. 4.5. Except for the first few responses (driving with the lowest frequencies) that have plane-wave like structure (Fig. 4.5(a-c)), the rest of the response patterns are similar and dominate at the system boundaries (representatives shown in Fig. 4.5(d-e)). This property is also clearly measured by the participation ratio of the response vectors, shown in Fig. 4.6(a) for three different system sizes and rhombic geometry. Namely, for most of the driving frequencies in the spectrum the response participation ratio defined in Section 4.3.4 is $P_R(\omega) \lesssim 0.3$ and decreases with the increasing system size, indicating a boundary

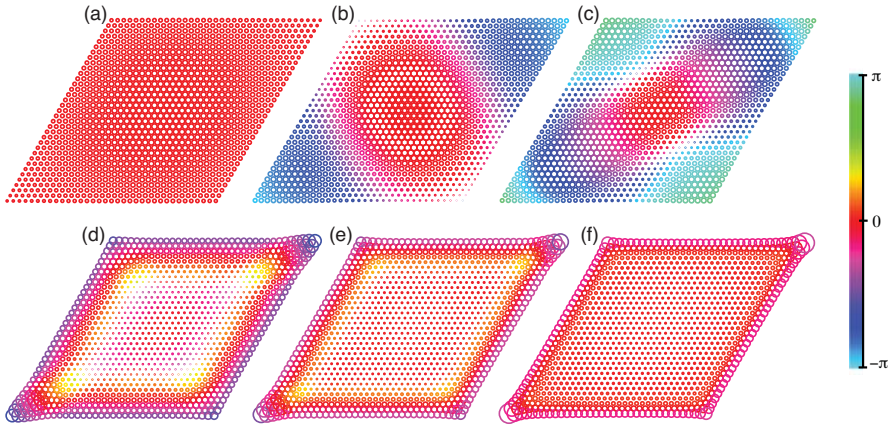

Figure 4.5: Response of the monodisperse 2D cluster of 1225 bubbles, when driven with (going from left to right in rows) the 1st, 3rd, 5th, 50th, 107th and 1107th resonant frequency. The radii of the circles around the bubble locations are proportional to the amplitude of the oscillation and the color shows the phase. Note how the response fields are featureless for driving above the lowest eigenfrequencies, due to both the overlap of many modes which washes out single-mode effects, and because modes with strong out-of-phase oscillations couple weakly to the uniform pressure driving, as discussed in Sections 4.2.4 and 4.2.5.

confinement[4]. The thickness of the boundary layer monotonically decreases with rising ω_d. This is clearly visible also in Figs. 4.5(d-f).

Figures 4.5(d-f) indicate an important clue for understanding the nature of these response fields. One can see that the majority of bubbles oscillate almost in phase with the driving. This leads to resemblance between the response and the uniform driving field, as captured by the upswing in the *response excitability*, Fig. 4.6(b) (introduced in Section 4.3.4). We find this behavior to be robust to introducing disorder. It is intriguing that in the experiments of [118], the observed oscillations resemble the low and high frequency response fields (the ones with high $\chi_R(\omega)$).

Mode excitability and contributions

We interpret the absence of extreme sensitivity on ω as it is seen in the mode participation ratio (cf. fig. 4.2) and the almost in-phase oscillation as a consequence of the excitation of many modes (as $ND(\omega)Q \gg 1$, see the explanation in Section 4.2.5). To illustrate this point, we analyze the eigenmode content of the response fields. According to Eq. (4.16), the eigenmode enters the response weighed by two factors: (*i*) the mode excitability (defined in Section 4.3.4) and (*ii*) its Lorentzian (*i.e.*, the mode reso-

[4] Obviously, these are not localized responses in the sense of Anderson localization (*i.e.*, due to disorder), but are corresponding to edge states in finite systems.

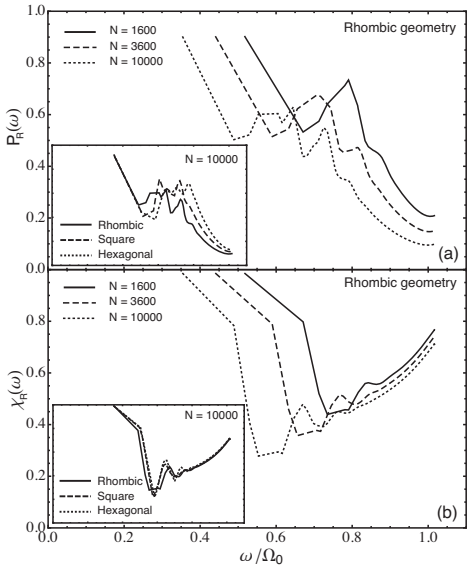

Figure 4.6: (a) Participation ratio of the response vs. scaled driving frequency for three different system sizes and rhombic geometry. Apparently localized response corresponding to driving with high frequency modes, is actually an edge response restricted to the system boundaries. The inset shows robustness of the behavior of the $P(\omega)$ to the change of the geometry. (b) Response excitability vs. scaled driving frequency for different cases as in (a). The response field resembles the uniform driving amplitude when the system is driven with the lowest frequency mode or with the modes at the high end of the spectrum. Inset shows the robustness to geometry change. In both (a) and (b) panels, data points are connected with lines for clarity.

nance curve) evaluated at the driving frequency. The normalized value of the first factor rapidly decays towards zero across the spectrum, except for the lowest mode for which it is normalized to one, Fig. 4.7(a)[5]. However, the resonance factor controlled by the mode Q-factor (see Section 4.2.1) singles out modes closest to the driving frequency. The final contribution of the eigenmodes is determined by an interplay of these two numbers; we plot characteristic outcomes in Fig. 4.7(b1-b4).

Due to its excitability, the lowest mode always contributes significantly, Fig. 4.7(b1-b4). However, the striking result is that since the density of modes is large (except for a few lowest, the rest $\sim N$ eigenmodes are clustered around the single bubble resonant frequency, Fig. 4.3(a)), the single mode resonance width (*i.e.*, the inverse Q-factor of the mode) is always large enough to allow many modes in the vicinity of ω_d to be excited (see already Section 4.2.1 and 4.2.5). This effect leads to cancellation

[5] Note that due to the symmetry, half of the modes are antisymmetric, and therefore have zero excitability.

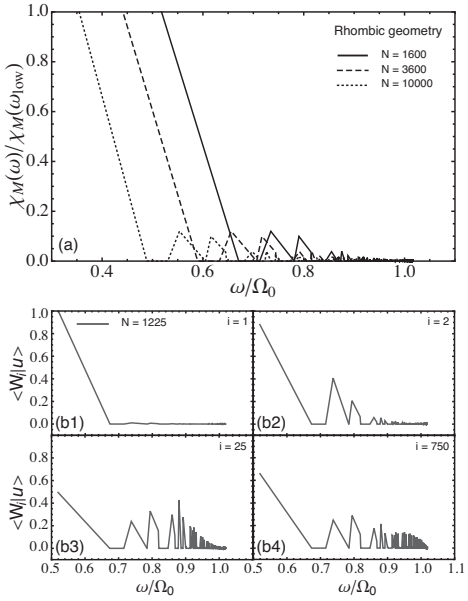

Figure 4.7: (a) Excitability of eigenmodes, normalized by the value for the lowest mode for three different system sizes and rhombic geometry. Note that for clarity data points between resonant frequencies have been connected by straight lines. Due to the symmetry, only half of the modes can be excited. Except for the lowest mode that resembles the driving amplitude, the excitability of the rest of the modes falls to zero quickly across the spectrum. This behaviour is robust to the change of the geometry (not shown here). (b1-b4) Eigenmode contributions to the typical responses for a system of $N = 1225$ bubbles and rhombic geometry. Considerable contribution of the lowest eigenmode is present in every response. When the system is driven with a frequency from within the peak of the density of states, many modes with resonant frequencies close to this value contribute almost equally to the response, (b4).

of detailed features of eigenmodes and to the "multi-mode" synchronized oscillation of bubbles in the response field. Fig. 4.7(b4) is a representative case, where the driving frequency falls inside the peak of the density of states, leading essentially to excitation of all the modes.

In terms of the sharpness of collective resonances (introduced in Section 4.2.5) and the mode density, the resonance width $D(\omega)/Q \sim D(\omega)\mu/\langle R_0\rangle$ needs to be $\lesssim 1/N$ for individual modes to be seen. In the presented data so far we did not include results with varying Q-factor (*i.e.*, bubble radii or viscosity) or interaction parameter K (*i.e.*, bubble radii or pitch). Indeed, the focus of this section was on varying system size and geometry, since the formalism presented in Section 4.3 is numerically simpler for the case of monodisperse bubbles, allowing us to study large systems and finite size

effects. We will vary Q and K for the more experimentally relevant case of disordered clusters in the next Section 4.5.

4.5 Results: Polydisperse bubbles on a lattice

After gaining understanding of the behavior of the "ideal" monodisperse case in the previous Section, we can proceed with introducing disorder into the system. As explained in the Introduction, the experimental parameter space is vast. The system is most sensitive to the changes of polydispersity of static bubble radii (Section 4.2.6), the sharpness of collective resonances (Section 4.2.1 and 4.2.5), and the interaction parameter (Section 4.2.2). In this Section we vary these parameters.

4.5.1 Weak disorder

To get an intuition of what happens to the spectrum of the 2D bubble cluster when we introduce polydispersity, we first draw static bubble radii from a Gaussian distribution with a small width of 1%. To be able to compare the results with the ones of the monodisperse case, the Gaussian distribution is centered around the parameters we have used in the previous section, namely the ambient radius $R_0 = 5\mu m$ and the bubble distance $d = 200\mu m$. All other parameters are fixed at the values of the previous sections. Beside introducing polydispersity, we will also vary Q and K, through varying the aforementioned parameters, and express them in the units of $Q_0 \sim R_0^{mono}/\mu^{mono}$ and $K_0 \sim R_0^{mono}/d^{mono}$. The data presented in this subsection are for systems of $N = 1225$ bubbles.

Spectrum

The main effect on the properties of the system, when disorder is introduced, is the appearance of (quasi)localized eigenmodes at the high-frequency end of the spectrum, Fig. 4.8(b) (black dashed curve). An example of a quasi-localized mode is given in Fig. 4.8(2) — from here on we refer to panels illustrating examples of eigenmodes or response as Fig. 4.8(2) etc. The value of 1% polydispersity is enough to localize a significant fraction of the eigenmodes. These quasi-localized modes have amplitudes concentrated on a group of bubbles, with some resemblance to the coherent waves of the monodisperse system.

At this point we can compare the influence of the three control parameters on the density of states. Compared to the monodisperse case Fig. 4.8(a) (black solid line), introducing the polydispersity broadens the density of states, Fig. 4.8(a) (black dashed line). The broadening is accompanied with a shift of the peak position towards frequencies below Ω_0 (this will become more obvious with the increase of polydispersity in the next subsection, Fig. 4.12(a)).

The Q-factor, *i.e.*, the width of the collective resonances, is not expected to influence the spectrum, *i.e.*, the positions of the collective resonances as long as Q is

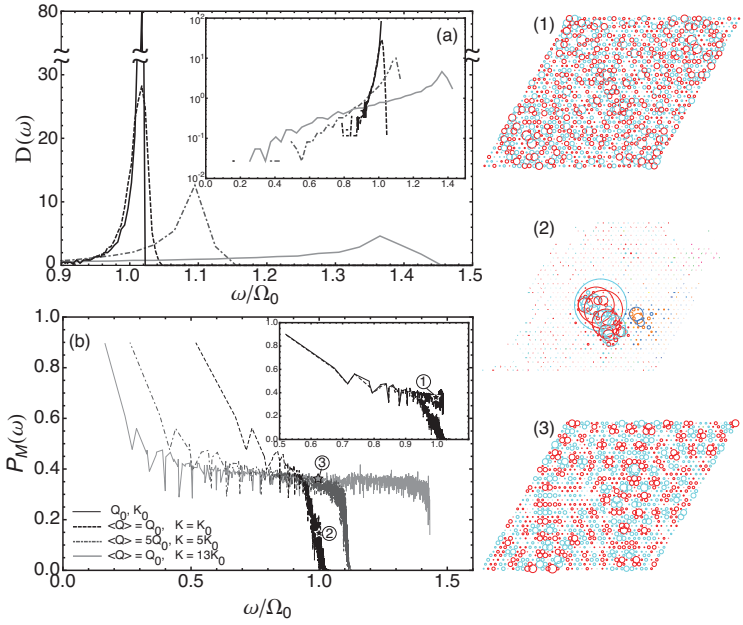

Figure 4.8: Spectrum, example modes, and mode participation ratio for systems with disorder: (a) Density of states for a system of $N = 1225$ bubbles. Initial bubble radii are coming from a Gaussian distribution with the width of 1%. Different curves are for different value of the interaction parameter: the black dashed curve is for parameters as in the monodisperse case (solid black line), but with 1% of polydispersity; the gray dash-dotted one is for the case of average bubble radii being five times bigger (this also increases the sharpness of the resonances, which by itself has negligible influence on $D(\omega)$); the solid gray line is for the case in which the interaction parameter K is thirteen times as strong. Note how the spectrum broadens once disorder is introduced. The inset shows the same data as in the main panel, but on a semi-log scale. (b) Mode participation ratio for systems as in (a). Even 1% of polydispersity localizes modes at the high-end of the spectrum. This effect is clearly seen in the inset of (b) where we plot P_M for the monodisperse (black solid line) and 1% polydisperse (dashed black line) cluster. To emphasize the effects of disorder, in (1) and (2) we are plotting examples of modes that have approximately the same eigenfrequency, $\omega/\Omega_0 \approx 1$ (marked in fig. 4.8b), but are either coming from the monodisperse (1) or 1% polydisperse (2) spectrum, respectively. Once K is increased (Section 4.2.2), localization gets suppressed, as captured with the solid gray line in (b). This can also be seen in the example mode (3) (again for $\omega/\Omega_0 \approx 1$), that starts to recover plane wave like behavior. In both the (a) and (b) panels, data points are connected by lines for clarity.

large. Indeed, a five-fold change of the Q-factor through increase of $\langle R_0 \rangle$ (with K kept constant by corresponding change of pitch d) introduces a negligible broadening of the DOS peak, which we therefore do not plot. (However, the Q-factor will become crucial for response.)

The interaction parameter K tends to shift the peak to higher frequencies while significantly broadening it, Fig. 4.8(a) (dash-dotted and solid line). The stiffening of the oscillators is due to the increased interaction strength, see also Section 4.2.2. Another consequence of the stiffening is the suppression of the localized eigenmodes at the high end of the spectrum, Fig. 4.8(b)(dot-dashed and solid line) and mode depicted in Fig. 4.8(3).

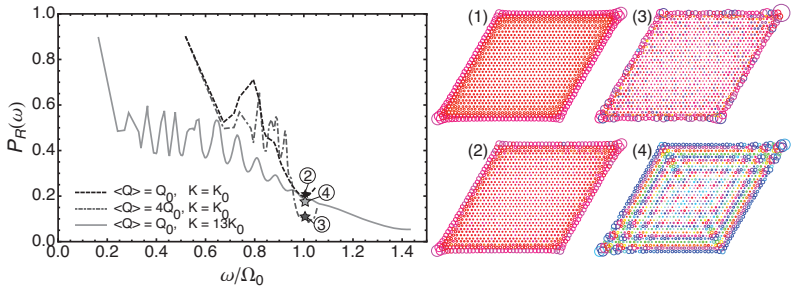

Figure 4.9: Main panel: Response participation ratio as a function of driving frequency for a system of $N = 1225$ 1% polydisperse bubbles. Panels (1-4) show response fields of different systems, driven with $\omega/\Omega_0 \approx 1$. For $\langle Q \rangle = Q_0$ and $K = K_0$ (see Section 4.4), black dashed line, $P_R(\omega)$ does not noticeably differ from the result of the monodisperse case. This can be seen when comparing panels (1) (response of the monodisperse system), and (2) (response of the 1% polydisperse system). Once we change $\langle Q \rangle$, through changing μ, and K, through changing d, oscillations in the plateau of $P_R(\omega)$ are introduced, which originate from P_M (Fig. 4.8(b)) and P_M^{mono} (Fig. 4.3(b)) respectively. This can also be seen in panels (3) and (4) where a response of systems with $\langle Q \rangle = 4Q_0, K = K_0$ and $\langle Q \rangle = Q_0, K = 13K_0$ respectively is plotted. In the main panel, data points are connected with lines for clarity.

The response fields strongly resemble the monodisperse case, with a mostly featureless edge character for driving at frequencies within the peak of the density of states (Fig. 4.9(2)), and a plane wave like shape for low-frequency driving. The presence of disorder manifests itself in slight random variation of the bubble oscillation phase in the response. Although the high frequency eigenmodes are progressively more localized towards the spectrum edge, the density of states remains high enough for effective damping to wash out features of the response to even the highest frequency driving.

Following the discussions in Section 4.2.5 and at the end of the previous Section, we expect that an increase of the Q-factor counteracts the tendency of effective

damping at a given density of states in the spectrum around the driving frequency. In other words, there is a shift towards a single mode response, as the weight is focused to fewer modes in the response (see Section 4.2.5). We indeed see in Fig. 4.9(3) that the edge like response fields obtain local features, resembling the eigenmode shapes. On the other hand, the increase of K introduces a plane wave like modulation (Fig. 4.9(4)), resembling the ideal system eigenmode shape. The increase of interactions between bubbles causes local out of phase ("optical-like", as standardly called in condensed matter physics) oscillations and weakens the effect of disorder.

Mode and response participation ratio

We also observe this change by analyzing the behavior of the mode and response participation ratios $P_M(\omega)$ and $P_R(\omega)$. In the mode participation ratio, $P_M(\omega)$, there are characteristic oscillations within the plateau (at $P_M \approx 0.4$), which are not sensitive to the change of the Q-factor and K. The main panel of Fig. 4.8(b) demonstrates this robustness to changes in both the Q-factor and the interaction parameter through the mean initial bubble radius $\langle R_0 \rangle$ (the curves have similar oscillation features, except for spanning different ranges in frequency). Looking at the response participation ratio $P_R(\omega)$ however reveals no oscillations when the Q-factor is kept at lower values, Fig. 4.9 (black dashed line). As the Q-factor is increased by changing μ (Fig. 4.9 gray dot-dashed line), the oscillations characteristic of the mode participation ratio $P_M(\omega)$ appear in the plateau of $P_R(\omega)$. This is a manifestation of the increasingly "single mode" nature of the response as the resonances are sharpened (*i.e.*, Q-factor increased). There is an increased resemblance of the response and eigenmode shapes at a given (driving-, and eigen-) frequency. On the other hand the increase of the interaction parameter produces the same end result of oscillations of P_R, but in a slightly different way: the response fields pick up the ideal system eigenmode shapes and consequently the oscillations from P_M of Fig. 4.4.

Frequency response and absorption

We now address the implications of our results on experimentally observable quantities. We therefore study both the frequency response ϵ_R and the absorption of the system, when driven uniformly with some frequency ω, taken to be in the range 0 to $3\Omega_0$. In Fig. 4.10(a) we show the frequency response for three different sets of values of Q and K. The pronounced peak in the case of $\langle Q \rangle = Q_0$ and $K = K_0$ (dashed black line) is the response positioned at the lowest frequency mode. This mode is the least damped one, and follows the uniform driving the most, therefore giving the strongest response. Inset shows a zoom-in of the main panel, where one can see a second, significantly smaller peak, corresponding to the response at the second lowest frequency mode. Once we increase the $\langle Q \rangle$ factor (dot-dashed gray line), existing peaks become more pronounced, and additional peaks appear (see inset) as is expected when the mode Lorentzians are narrower. As we have learnt from the density of states of the system with increased interaction parameter K (Fig. 4.8(a)), the spectrum becomes

broader and stretches to lower frequencies, therefore shifting the response peak.

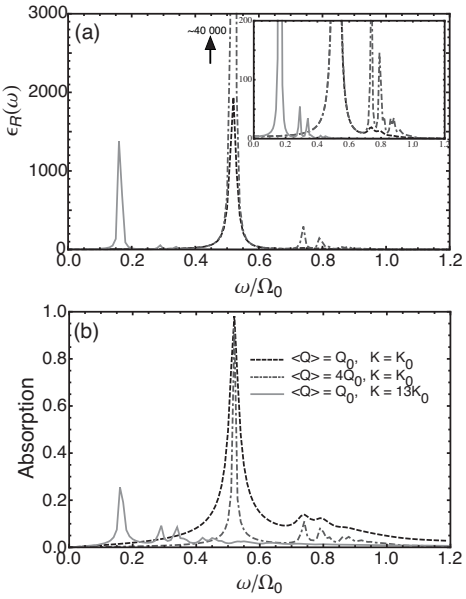

Figure 4.10: (a) Frequency response of the system of $N = 1225$, 1% polydisperse bubbles to uniform driving. Contrary to previous plots, where data points at resonant frequencies are connected by straight lines, here the frequency is varies continuously. The pronounced peak in the case of $\langle Q \rangle = Q_0$ and $K = K_0$ (dashed black line) is the response at the lowest frequency mode. Inset shows a zoom-in of the main panel, where one can see a second, significantly smaller peak, corresponding to the response at the second lowest frequency mode. Once we increase the $\langle Q \rangle$ factor (dot-dashed gray line), existing peaks become more pronounced, and additional peaks appear (see inset) as expected. Increasing interaction parameter K stretches the spectrum, and therefore moves the resonant peaks to lower frequencies, at the same time lowering their intensity. (b) Absorption, defined as the time averaged dissipated energy under driving for systems as in (a).

The absorption gives the time averaged dissipated energy under driving. When driving is at resonant frequency of a mode, that mode contributes to absorption proportionally to its damping coefficient and the overlap between the mode and the uniform driving vector (cf. Section 4.3.3). In Fig. 4.10 (b) we show the absorption curves for three different sets of values of Q and K as in (a). Although intuitively one expects high absorption for the modes with highest damping, which is the case for the highest-frequency modes of the system, we find the highest absorption around the lowest resonance, which is weakly damped but has the largest overlap with the uniform driving (dashed black curve). Increase of the sharpness of the resonances lowers

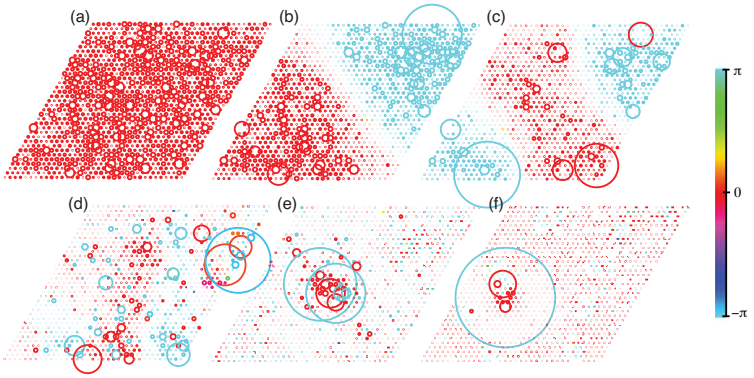

Figure 4.11: Six eigenmodes of the undriven, 20% polydisperse 2D bubble cluster. For this illustration we chose (going from left to right in rows) the 1st, 3rd, 5th, 107th, 507th and 1107th mode of the system with 1225 bubbles in rhombic geometry. The radii of the circles around the bubble location are proportional to the amplitude of the oscillation and the color shows the phase. Note the strong Anderson-like localization of the eigenmodes.

the damping and therefore the absorption (dot-dashed gray line).

4.5.2 Strong disorder

In this subsection we present results for the case of strongly disordered bubble clusters on a lattice, where we impose 20% of polydispersity in initial bubble sizes. At this level of disorder, Anderson localization of modes is dominant and has a strong impact on the response to driving. The main effects of strong disorder on the response, that we present in this subsection, are the appearance of *quasi-localized* low-frequency and high-frequency modes and *optical-like* delocalized high-frequency modes.

Spectrum

Demonstrative examples of eigenmodes in the presence of strong disorder are shown in Fig. 4.11. In the lowest frequency modes of Fig. 4.11(a-c) the underlying plane wave like pattern is still visible with an addition of a few strongly oscillating bubble groups, constituting a so-called quasi-localized mode. The rest of the spectrum is populated with very localized or quasi-localized modes, typical examples of which are shown in Fig. 4.11(d-f). The mode participation ratio, presented in Fig. 4.12(b), captures the localization behavior well. Even the lowest modes show $P_M \lesssim 0.4$, whereas most of the spectrum has $P_M \sim 1/N$, *i.e.*, is localized on the single bubble level. The interaction parameter K induces the same qualitative change as in the low disorder case, suppressing localization (less effectively in the high-end tail of $D(\omega)$).

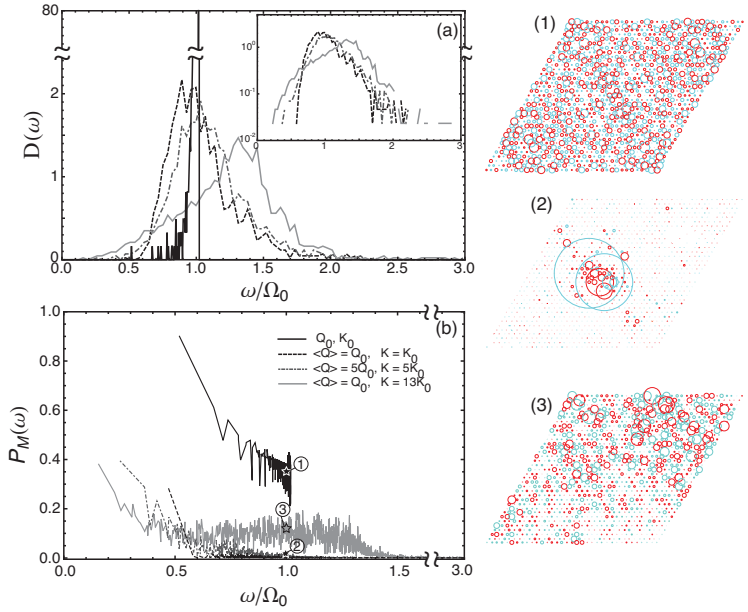

Figure 4.12: Spectrum, example modes and mode participation ratio for systems with disorder: (a) Density of states for a system of $N = 1225$ bubbles. Initial bubble radii are coming from a Gaussian distribution with the width of 20%. Different curves are for different value of the interaction parameter: the black dashed curve is for parameters as in the monodisperse case but with 20% of polydispersity; the gray dash-dotted one is for the case of average bubble radii being five times bigger (this also increases the sharpness of the resonances, which by itself has negligible influence on $D(\omega)$); the solid gray line is for the case of pitch decreased ≈ 13 times. For comparison we also included $D(\omega)$ of the monodisperse system, solid black line. Note how the spectrum broadens with the increase of disorder. The inset shows the same data as the main panel on a semi-log scale, with the monodisperse system omitted. (b) Mode participation ratio for systems as in (a). 20% of polydispersity localizes almost all modes (dashed black line) compared to the monodisperse case (solid black line). To emphasize the effects of disorder, in (1) and (2) we are plotting examples of modes that have approximately the same eigenfrequency, $\omega/\Omega_0 \approx 1$, but are coming from the monodisperse and 20% polydisperse spectrum respectively. Once K is increased (Section. 4.2.2), localization gets suppressed, as captured with the solid gray line in (b). This can also be seen in the example mode (3) (again for $\omega/\Omega_0 \approx 1$), that starts to recover plane wave like quality. In both (a) and (b) panels, data points are connected by lines for clarity.

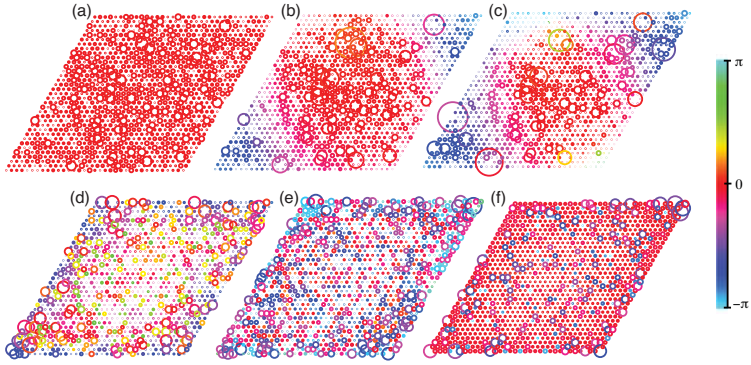

Figure 4.13: Response of the 20% polydisperse 2D cluster of 1225 bubbles, when driven with (going from left to right in rows) the 1st, 3rd, 5th, 107th, 507th and 1107th resonant frequency. The radii of the circles around the bubble locations represents the amplitude of the oscillation and the color shows the phase. Examples (b) and (c) are good representatives of the quasi-localized response fields, and (f) shows an example of a delocalized optical-like high-frequency response.

As mentioned in the previous subsection, the density of states differs significantly from the monodisperse case, Fig. 4.12(a). The previously sharp single bubble resonance peak (solid black line) becomes wide, and somewhat shifts to lower frequencies (dashed black line). A long tail appears in the $D(\omega)$ up to $3\Omega_0$, sparsely populated by very localized modes — an example of a quasi-localized mode is depicted in Fig. 4.12(2). The increase of the interaction between the bubbles and sharpness of the resonances parameters induce the same qualitative changes as in the low disorder case. Localization and quasi-localization of the modes is captured by the P_M, Fig. 4.12(b). Compared to the monodisperse case (solid black line and example mode depicted in Fig. 4.12(1)), 20% of polydispersity localizes all the modes, dashed black line and example mode depicted in Fig. 4.12(2). Once the interaction parameter is increased, like in the low-disorder case, modes start to recover the plane-wave like character (Fig. 4.12(3)).

Response fields and response participation ratio

In the response fields, Fig. 4.13, there is a recognisable underlying pattern similar to the low-disorder case (plane-wave and edge like response), on top of which there is a large number of single bubble oscillations with rapidly fluctuating phases. This can be understood as an effect of the broadening of the density of states, which causes the mechanism of effective damping to be less efficient, Fig. 4.15. The fluctuating phase pattern that appears in the response field is then due to the underlying eigenmode. A consequence of the observations above is that the response fields show localization. This is manifested in the calculated participation ratio, which is plotted in Fig. 4.14

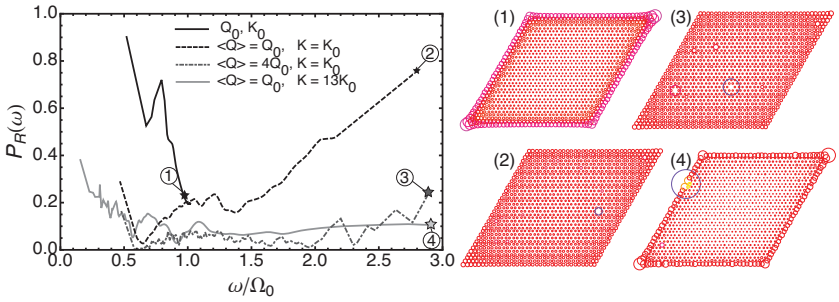

Figure 4.14: Response participation ratio of a system of $N = 1225$, 20% polydisperse bubbles. Response to driving with frequencies within the peak of the now broad $D(\omega)$ is localized, while $P_R(\omega)$ increases for high-frequency driving (dashed black curve), where the modes are sparse and effective damping suppressed (response to driving with the highest frequency is shown in (2)). Once K or Q are increased (dash-dotted and solid gray line, respectively), the high-frequency response becomes localized, but in different ways, see main text. The effect on the highest resonant frequency driving is shown in (3) and (4). The solid black curve shows the data for the monodisperse system as a comparison. In the plots, data points are connected by lines for clarity.

(dashed black curve). It is interesting to note that in the eigenmodes the disorder produces a large variation of amplitudes as well as phases at the single bubble level, while in the response fields it is mostly the phase that significantly fluctuates.

A surprising feature is that the above explanations fail in the case of highest driving frequencies, where the response becomes *delocalized* (as in Fig. 4.13(f) and Fig. 4.14(2)). We can however understand this by observing that the highest part of the spectrum $\Omega \lesssim \omega \lesssim 3\Omega$ is very sparse, containing just a few modes. This allows the lowest mode, which is off-resonance but has $\langle P|u_i\rangle \sim 1$, to dominate the contribution of the very few highest near on-resonance eigenmodes, which have $\langle P|u_i\rangle \sim 0$. As we increase the Q-factor, the highest frequency modes become more localized, giving a more localized response. With increased interaction parameter, the response shifts towards the monodisperse response, with a pronounced edge-like structure.

Response excitability and mode contributions

The basic influence of the sharpness of the individual resonances and interaction parameter of bubble-bubble interactions parameters is qualitatively the same as for low disorder. In this case, increasing any of the two leads to localization of the highest driving frequency responses, albeit through different mechanisms, Fig. 4.14. With increasing sharpness, *i.e.*, increase of the resonance factor for the highest modes, the contribution to response shifts away from the lowest mode, Fig. 4.15(b). The response becomes quasi-localized, resembling the highest eigenmode coupled to a uniform background. On the other hand, increasing K causes the system to behave more sim-

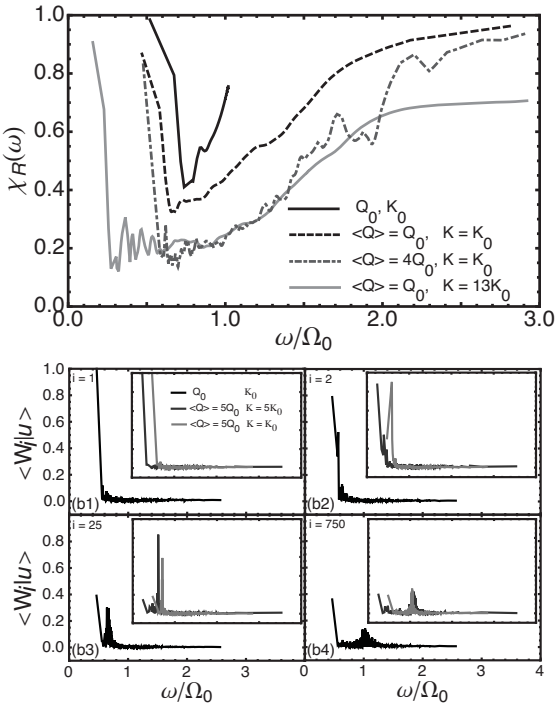

Figure 4.15: (a) Response excitability of a system of $N = 1225$, 20% polydisperse bubbles. For most of the driving frequency range, χ_R behaves as in the low-disorder case (black solid line). As we drive the system with highest eigenfrequencies, response starts to look like the uniform driving field considerably. Increasing Q localizes the response, hence reducing the resemblence to the driving. (b) Eigenmode contributions to the typical responses. Compared to the low-disorder case, the contribution of the lowest eigenmode is not significantly higher in every response. When a system is driven with a frequency within the now broad peak of $D(\omega)$, a number of modes $\ll N$ gets excited (*i.e.*, effective damping is less efficient), making the eigenmodes more visible in the response. Insets show the influence of the Q-factor and K parameters. In both (a) and (b) panels, data points are connected with lines for clarity.

ilarly to the ideal system (see also the discussion in Section 4.5.1), and the response acquires the familiar edge shape along some local disorder events, again leading to localization, but of the edge type. The plot of response excitability, Fig. 4.15(a), shows that the highest driving response resembles the inform driving field the most (dashed black curve), but localizes at higher values of K or Q.

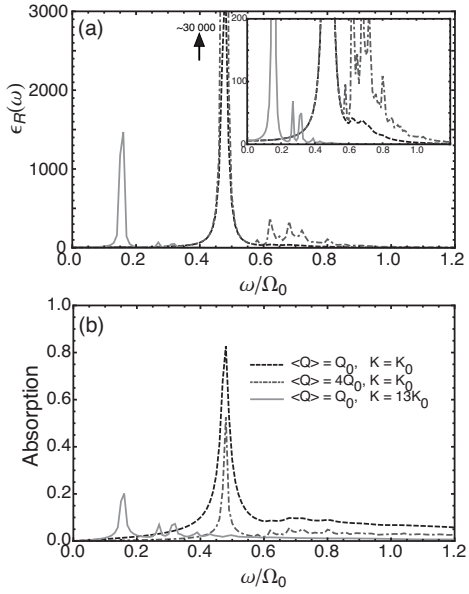

Figure 4.16: (a) Frequency response of the system of $N = 1225$, 20% polydisperse bubbles to uniform driving. The pronounced peak in the case of $\langle Q \rangle = Q_0$ and $K = K_0$ (dashed black line) is the response at the lowest frequency mode. Inset shows a zoom-in of the main panel, where one can see a second, significantly smaller peak, corresponding to the response at the next few lowest frequency modes. Note that the ratio of the primary and secondary peak heights is smaller here than at low disorder (Fig. 4.10). Once we increase the $\langle Q \rangle$ factor (dot-dashed gray line), existing peaks become more pronounced, and additional peaks appear (see inset) as expected (More peaks appear than at low disorder, inset of Fig. 4.10(a), since here the modes are more sparse). Increasing interaction parameter K stretches the spectrum, and therefore moves the resonant peaks to lower frequencies, at the same time lowering their intensity. (b) Absorption, defined as the time averaged dissipated energy under driving for systems as in (a).

Frequency response and absorption

Fig. 4.16 shows the frequency response and the absorption (Section 4.3.3) results for the strongly disordered systems. The essential features are interpreted in the same way as for the low disorder case, Section 4.5.1. The higher amount of polydispersity however explicates two main effects of disorder. Firstly, the low density of modes at lower frequencies is responsible for the appearance of more pronounced secondary peaks in the frequency response, (Fig. 4.16(a)). Secondly, the relative intensity of the primary and secondary peaks changes considerably. At 1% polydispersity the ratio was around 100, while in the present case of 20% polydispersity it is lowered to around

60. This parameter is easily accessible to experiments, and was considered in the analysis of micromeniscus oscillations [123], where the numerical model predicted a much higher ratio than found in the measurement data. In that work, disorder is not explicitly taken into account, while our results suggest it may be a decisive factor. The overall absorption becomes lower with the introduction of more disorder, Fig. 4.16(b).

4.5.3 Exponential vs. power-law localization

Let us finish this Section with a more detailed analysis of the subtle issue of whether we observe true *exponential* Anderson localization or a *power-law* like quasi-localization. Exponential localization is typical for systems with local interactions, whereas for the bubble clusters analyzed in this Chapter the pressure-mediated interactions fall off inversely with distance, *i.e.*, are long-ranged.

For illustrative purposes, we also simulated bubble clusters with the same parameters as in Section 4.5.2 (*i.e.*, 20% polydispersity), but now artificially cutting off all long-range interactions, thus allowing only for the nearest neighbor interactions. In order to see the quantitative effect of different interactions on the eigenmodes, we analyze the squared amplitude of each bubble, $|u_i|^2$, as a function of its radial distance from the maximal amplitude bubble in the mode, for both short- and long-range interaction.

Fig. 4.17 summarizes our findings: In (a) we plot the highest frequency mode of a cluster with a long-range interaction, and observe a power-law behavior. For comparison, in the inset we plot both the mode from the main panel and the highest frequency mode of a cluster with a short range interaction. The difference between the exponential and the power-law localization is captured well. In (b), variables that we plot are the same as in (a), only the mode that we study has an eigenfrequency close to the single bubble resonant one.

As can be seen in the main panels of Fig. 4.17, the scaling exponent we observe varies from mode to mode and even within one mode due to the large scatter. Naïve analysis, that takes into an account only the fact that the bubbles interact like $1/r_{ij}$, would give $|u_i|^2 \sim 1/r^{-2}$. However, our modes rarely have only one bubble carrying the oscillation: most of the time we have groups of a few bubbles oscillating strongly, with differing phases. As an example, if maximal oscillation occurs for two bubbles which have opposite phases, a bubble far from them would essentially feel a *dipole* interaction. If this would be the case, one should observe $|u_i|^2 \sim 1/r^{-4}$. We believe that our results reflect a combination of the two behaviors.

In the end let us mention the interesting question of when and how does the transition from exponential to power-law localization happen. Previous theoretical and numerical studies find Anderson localization of acoustic energy in bubbly liquids in a narrow frequency range around single bubble resonant frequency [126, 127]. At similar disorder strength we find power-law localization of modes at similar frequencies. Within our approach focused on bubble oscillations we trace back the different nature of localization to $1/r$ interaction [116, 121, 122].

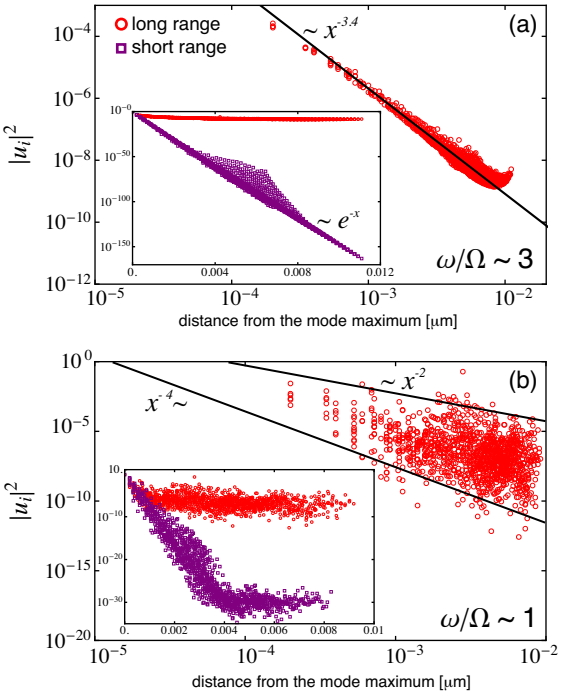

Figure 4.17: Quantitative comparison of the falloff of the amplitude $|u_i|^2$ of the eigenmodes as a function of distance r from the bubble with the largest oscillation amplitude, of clusters with a long- and short-range interaction. Both clusters have $N = 2025$, 20% polydisperse bubbles. (a) Log-Log plot of the highest frequency mode of a cluster with a long-range interaction. Power-law localization can be clearly seen. Inset compares the mode plotted in the main panel, with the highest frequency mode of a cluster with a short-range interaction. We use Log-Linear scale to emphasize the exponential behavior of the latter mode. (b) As in (a), only comparing modes with an eigenfrequency close to the single bubble resonant frequency.

4.5.4 Polydisperse bubbles on a random underlying structure

As noted in the introduction, the case of random underlying structure is relevant for experimental 3D systems. In this section we consider random bubble positions, drawn from a uniform distribution. We discard bubbles that have neighbours closer than $3\langle R_0\rangle$ and limit ourselves to 20% polydispersity.

We find that all the conclusions and analysis of the results for this case are qualitatively the same as in the case of 20% polydisperse bubbles on a lattice, considered in the preceding subsections. To avoid repetition, we omit plots of the relevant quantities. Mode and response fields are shown in Figs. 4.18 and 4.19, and are analogous to Figs. 4.11 and 4.13.

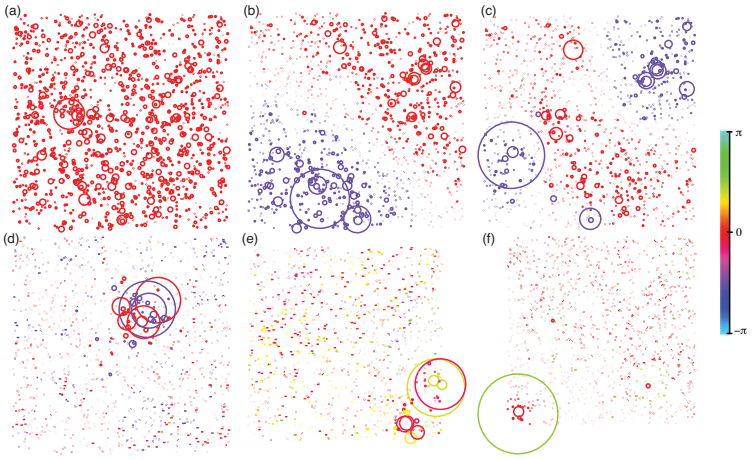

Figure 4.18: Six eigenmodes of the undriven, 20% polydisperse 2D bubble cluster on a random underlying pattern. For this illustration we chose (going from left to right in rows) the 1st, 3rd, 5th, 107th, 507th and 1107th mode of the system with 1225 bubbles in square geometry. The radii of the circles around the bubble locations is proportional to the amplitude of the oscillation and the color indicates the phase. Note the strong Anderson-like localization of the eigenmodes.

The main quantitative difference, brought by the random underlying structure, is observed in Fig. 4.18(b,c). Namely, the quasi-localized character of the modes is more pronounced, due to the fact that occasionally bubbles can be close to each other, taking the role of a single, relatively large bubble.

4.6 Outlook on experimental verification

The present Chapter has presented the results of a theoretical analysis, but one of course wonders what features could directly be confirmed in experiments. To address this question we come back to the experiments of [118, 119] and [123] which had motivated the present study. In both of these studies the collectively responding bubbles (or menisci) were fixed in space to a two-dimensional array. Such geometrical constraint indeed eases the visualization of the bubble oscillations. The two most prominent collective features may be the existence of the pronounced edge states which first had been seen by [118] and the pronounced low-frequency response as seen by [123]. We suggest to study how these collective features evolve with increasing bubble number N. Moreover, we suggest to study how more *localized* modes evolve once disorder is introduced through a more polydisperse bubble size distribution. It would also be interesting to observe how the increase of viscosity affects the mode response and how the theoretical prediction – an enhanced multi-mode response –

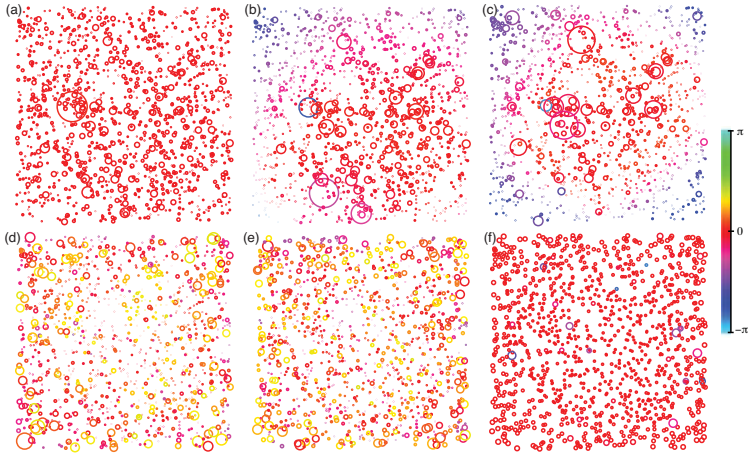

Figure 4.19: Response of the 20% polydisperse 2D cluster of 1225 bubbles on a random underlying pattern, when driven with (going from left to right in rows) the 1st, 3rd, 5th, 107th, 507th and 1107th resonant frequency. The radii of the circles around the bubble locations represent the amplitude of the oscillation and the color the phase.

materializes in the experiments.

Though experimental observation may be easiest for 2D bubble configurations, an extension to the 3D case is possible: [133] succeeded to trap bubbles with optical tweezers and exciting these bubbles with an acoustic field is clearly feasible. Presently however one is constrained to a few bubbles only, due to the technical complications.

Also the case of freely moving bubbles in 3D in an acoustical field is becoming experimentally accessible, thanks to the tremendous progress in 3D particle tracking velocimetry [134, 135]. [136] have recently extended these methods to the tracking of thousands bubbles. However, the obstacle still to be taken here is to provide sufficient spatial resolution to monitor the volume oscillation of each individual bubble. Due to the Bjerknes forces of first and second kind [116] the bubbles in an acoustic field organize in bubble streamers [73, 121, 122, 137], leading to a highly inhomogeneous bubble distribution in space.

For collectively oscillating bubble in 3D the experimentally most accessible quantity may be the absorption spectrum, as shown in figures 4.10b or 4.16b. Again, one can only expect to identify general features and trends with control parameters such as with the total number of bubbles or with the viscosity.

In any case, bridging the gap between the present theoretical analysis of collectively (linearly) oscillating bubbles in either two or three dimensions and real world experiments is still a major task ahead of us, but we are convinced that the present analysis has identified striking and often surprising effects which are – as pointed out and examplified in the Introduction – very relevant for various phenomena in nature

and technology.